JOURNAL OF MATERIALS SCIENCE 23 (1988) 2195–2204

Oxidizing heat treatment of nickel embedded in a barium titanate ceramic: kinetics and mechanisms of the metal oxidation

J. WEISS*
Philips GmbH, Forschungslaboratorium Aachen, Weisshausstrasse, D-5100 Aachen, West Germany

The use of nickel electrodes in combination with donor-doped $BaTiO_3$ for ceramic multilayer capacitors was investigated. Their use requires a reducing sintering atmosphere in order to maintain the metallic state. Afterwards such devices have to be exposed to a short oxidizing heat treatment in order to transform the semiconducting ceramic into the insulating state. The results show, that from the kinetics such a treatment would be possible with the diffusion in a newly formed NiO layer being the rate-controlling step at 1000° C. However, the multilayer geometry and the fact that the oxidation of nickel consumes far more oxygen than the transformation of the ceramic from the semiconducting into the insulating state, do not allow the use of nickel electrodes in combination with a donor-doped $BaTiO_3$ ceramic.

1. Introduction

The fabrication of ceramic multilayer capacitors (CMC) based on donor-doped barium titanate requires the use of expensive palladium or Pd–Ag electrodes in order to sinter them in an oxidizing environment. Their substitution by cheaper nickel electrodes requires a reducing sintering atmosphere in order to inhibit metal oxidation. Then the defect chemistry of the ceramic, which has been studied intensively [1–5], necessitates the use of acceptor dopants in order to maintain the insulating state in the $BaTiO_3$ dielectric, which otherwise would become semiconducting.

The use of an acceptor-doped barium titanate is not desirable for a number of reasons.

1. Development of such a material for all temperature specifications is costly and time consuming.
2. The relative permittivity of such materials is generally lower than that of donor-doped ones and in turn the dissipation factor in the latter is higher [6, 7].
3. Insulation resistance and degradation behaviour of donor-doped materials is superior to that of acceptor-doped ones [8, 9].

The purpose of the present investigation was to find out whether the use of nickel electrodes in combination with a donor-doped material would be possible in order to overcome these problems. Theoretically such a possibility exists, when the multilayer capacitors are sintered under reducing conditions with a rapid oxidizing reheating, such that it transforms the ceramic into the insulating state without any severe oxidation of the embedded nickel electrodes.

For the study of the mechanisms controlling the reoxidation of the ceramic and the oxidation of the nickel, simple geometries of ceramic–metal couples were used at first. Then multilayer capacitors were studied in order to see possible effects of geometry and find out the applicability of such a process. In starting such an investigation the extensive knowledge about the defect chemistry of $BaTiO_3$ [1–5] and NiO [10–15], that will form as an oxide layer on the nickel electrodes, is used together with data on diffusion in these compounds [12–18]. These data describe diffusion in $BaTiO_3$ by transport via oxygen vacancies, $V_O(BT)$, in $BaTiO_3$ in the whole oxygen partial pressure range. For NiO, nickel vacancies, $V_{Ni}(NiO)$, are the fastest diffusing species [14]. It is unique for both diffusion mechanisms, that they are controlled by the gradient of the chemical potential of oxygen, which is for simplification expressed by the equivalent oxygen partial pressure, p_{O_2}, throughout the text.

2. Experimental procedure

2. 1. Sample preparation

In order to check the parameters of the rate-controlling step and the geometry, two types of samples were prepared: (1) for the determination of the rate-controlling step in the oxidizing heat treatment, $BaTiO_3$ powder was pressed in a steel die with steel plungers to cylinders of 10 mm diameter and roughly 10 mm length. These cylinders were slightly sintered at 1000° C, 1 h in air in order to ensure sufficient mechanical stability. Then a hole of 1.1 mm was drilled along the cylinder axis and a 1 mm nickel wire was inserted, sticking out somewhat at both ends. This assembly was sintered at 1350° C, 4 h in moisted N_2–5% H_2 which yielded a dense ceramic with few remaining pores and a tightly fitting nickel wire. Finally the two ends of the cylinder were covered with Ni : NiO paste (20 : 80 wt %) and burnt in at 1200° C for 2 h in moisted N_2–5%H_2. This produced a dense nickel layer at the ends. Thus only radial diffusion upon the oxidizing heat treatment was possible. (2) The multilayer

Present address: Renker GmbH, Hausener Weg, D-7800 Freiburg, West Germany.

0022–2461/88 $03.00 + .12

TABLE I Chemical analysis

(a) Ni 99.2, supplier VDM no. 2.4066, analysed by spectroscopy

Element:	Co	Cu	Fe	Mn	Si
Wt %	0.03	0.1	0.02	0.2	0.03

Al, Cr, Mg, Mo, Ta, Ti below 0.01 wt %

(b) $BaTiO_3$, supplier Tamtron, Niagara, USA

Pure $BaTiO_3$ (type Tam HPB = $Ba_{100}Ti_{100.6}O_{301.2}$)

Element	Ca	Sr	Na	Rb	Co	Si*	Fe*	Al*	Mg*	Nb*	Co*
Wt p.p.m.	21.6	103	13	42	42	0.003	0.002	0.003	0.0004	< 0.02	< 0.001

NbCo-doped $BaTiO_3$ (type Tam Bx lot 1009)

Element	Ca	Sr	Na	Rb	Cl	Si*	Fe*	Al*	Mg*	Nb*	Co*
Wt p.p.m.	34	290	77	–	–	0.003	0.002	< 0.0006	0.0004	1.54	0.33

Element	Ba	Ti
Wt %	56.6	19.8

*Wt %.

capacitors were prepared by the standard process by foil casting with subsequent screening of the electrodes and stacking the foil [19, 20]. The thickness, d_e, of the dielectric layer was varied by stacking different numbers of foil in a range $25\,\mu m < d_e < 125\,\mu m$. The thickness of the cover layer, d_c, was also varied in the range $50\,\mu m < d_c < 375\,\mu m$. The CMCs were sintered dense, using the same conditions as for the cylinders.

Two different $BaTiO_3$ compositions were used for this investigation: pure $BaTiO_3$ with a minimal titanium excess and an NbCo-doped $BaTiO_3$. The chemical analysis of these materials and of the nickel wire is given in Table I together with the supplier.

2.2. Heat-treatment under oxidizing conditions

The oxidation treatment in air was performed in a platinum-wound furnace that could reach 1400° C within 10 min and had a cooling time of about 30 min. The treatment was done at three different temperatures (700, 1000, 1300° C) over various lengths of time. The long term treatments at 700° C ($t > 12$ h) were done in a canthal-wound pipe furnace, that was pushed over an open quartz pipe for rapid heating and cooling. In order to compare the oxidation measurements of the cylinders, three pieces of blank nickel wire were exposed to the same treatment.

Thermal mismatch and volume changes can have erroneous effects on such experiments by altering the oxidation mode of nickel. The thermal expansion coefficient, λ, is $12.9 \times 10^{-6} K^{-1}$ for nickel [10], $17.2 \times 10^{-6} K^{-1}$ for NiO [21] and $16.5 \times 10^{-6} K^{-1}$ for $BaTiO_3$ [22]. Sintering at 1350° C should thus result in a gap after cooling. This, however, was never observed; instead the nickel wire was still tightly fitting after all heat treatments. The volume change by oxidation from nickel (density $8.91\,g\,cm^{-3}$) to NiO (density $6.82\,g\,cm^{-3}$) in the cases of longer oxidation times resulted in an elongation of the nickel wire due to plastic flow. The size of the elongation was in the micrometre range and as such somewhat less than an estimated value by the volume change. In a few cases the pressure was strong enough to break the ceramic. Such samples were excluded from further investigation. In addition, a hole of 1.1 mm was drilled into one cylinder by ultrasonic drilling. Then the 1 mm nickel wire was inserted, fitting loosely in the hole. This arrangement was oxidized and upon longitudinal sectioning showed clearly stronger oxidation towards the ends of the cylinder than in the middle due to the geometry. The normally treated cylinders showed an even thickness over the entire length except for one treated at 1300° C, where the nickel cover layer was totally oxidized. These results make a direct vapour phase oxidation highly unlikely.

While oxidation of cylindrical samples was only performed in air, the multilayers were treated either in air or in technical N_2 with a $\log p_{O_2}$ of -4.5 bar.

2.3. Analysis of the oxidized samples

All cylindrical samples were cut at half length, perpendicular to the axis and ground and polished. The thickness of the NiO layer formed, d_{NiO}, was determined by optical microscopy. In most cases for one condition, two or three cylinders were analysed from optical micrographs at four locations rotated by 90° and using both halves. The same was performed on the blank nickel wires, which additionally were weighed before and after heat treatment. This more accurate means of analysis could not be carried out with the cylindrical samples, because the ceramic and the cover layer also contribute to the weight change. The layer thickness, d_{NiO}, served to calculate the oxidation constant, K, and compare the result with literature values [10, 22, 23]:

$$d d_{NiO}/dt = K/d_{NiO} \quad (1)$$

The constant K may be transformed into the usual dimensions ($g^2\,cm^{-4}\,sec^{-1}$) by multiplying d_{NiO} by the density of NiO. This allows us to determine the activation energy of the oxidation by the slope of the least squares fit in the $\ln K$–$1/T$ representation, which was done with samples oxidized for 2 h in air at temperatures from 950 to 1300° C in 50° intervals.

The CMCs were cut, ground and polished in the middle parallel to the end terminations. Here the oxidation process could only be evaluated in a qualitative manner which, however, clearly shows the influence of geometry for this process.

2.4. Chemical analysis

The impurity content of the nickel wire (Ni 99.2) was analysed by spectroscopy. Several of the cylindrical samples with various treatments were analysed by SEM and microprobe in order to study diffusion of nickel into the ceramic and to study diffusion of barium and – in the case of doped $BaTiO_3$ – niobium and cobalt into NiO or the metallic nickel. In one case an oxidized cylinder was treated under reducing conditions again, in order to show such interdiffusion effects between $BaTiO_3$ and NiO/Ni more clearly.

3. Results and discussion

The results of the experimental investigation are presented and discussed in this section in order to evaluate the mechanisms which control the oxidation of both the ceramic and the nickel embedded in it. Before doing this, the effect of the phase equilibria and of the interface reactions is discussed on a more theoretical basis.

3.1. Phase equilibria between $BaTiO_3$ and Ni/NiO

Knowledge of the phase equilibria in the system Ba–Ti–Ni–O is rather incomplete [25–27]. It is, however, a prerequisite in order to see which reactions are possible or impossible. There is a phase equilibrium between $BaTiO_3$ and nickel as well as a phase equilibrium between $BaTiO_3$ and NiO. The latter was checked by heat treating mixtures of both (50 : 50 mol %) compounds over 24 h at 1400° C in air, revealing just $BaTiO_3$ and NiO by X-ray diffraction and optical microscopy. The microprobe results, which will be discussed in further detail in a later section, show that no barium or titanium dissolves in NiO, while only up to about 1 mol % nickel dissolves in $BaTiO_3$. Consequently, the Ni–NiO equilibrium is not markedly influenced by the presence of $BaTiO_3$ and hence the phase boundary between nickel and NiO is, for a given temperature and ambient pressure, determined by the equilibrium oxygen partial pressure $p_{O_2}^{eq}$ of the reaction [10–15]

$$Ni + 1/2\ O_2 = NiO + V_{Ni}(NiO) \qquad (2)$$

with a reaction constant K_3 (numbered according to the sequence of interfaces given in Fig. 1) of:

$$K_3 = V_{Ni}(NiO)\, p_{O_2}^{-1/2} \qquad (2a)$$

Fig. 2 gives a schematic view of the influence of p_{O_2} on the compatibilities of the solid phases $BaTiO_3$, NiO and nickel, corresponding to the p_{O_2} of the vapour phase. The latter is not included, but under equilibrium conditions the p_{O_2} of the vapour atmosphere is directly related to the concentration of nickel vacancies in NiO as stated in equation 2 and to the concentration of oxygen vacancies in $BaTiO_3$ $V_0(BT)$ [1–5], which can be expressed by

$$V_0(BT) + 1/2\ O_2 = O(BT) \qquad (3)$$

yielding the reaction constant K_1

$$K_1 = V_0(BT)\, p_{O_2}^{1/2} \qquad (3a)$$

It is important to bear in mind, that nickel and the Ni–NiO interface for the oxidizing conditions encountered in these investigations have the lowest equivalent p_{O_2}, fixed by $p_{O_2}^{eq}$ defined by equation 2.

3.2. Reaction at the interface $BaTiO_3$–NiO

While reactions at interface 1 (gas–$BaTiO_3$) and at interface 3 (NiO–Ni) are discussed extensively in the literature [1–3, 10, 28], for the reaction at interface 2 ($BaTiO_3$–NiO) no literature results can be found. There are rather few data [29–31] on such solid–solid interface reactions available, and a unique feature of the reactions described there in detail is that one of the reactants is incorporated into the other upon the reaction. This is not the case here, when the marginal solubility of NiO in $BaTiO_3$ is neglected. Instead oxygen passes through without altering the two reactants. Using Equations 2 and 3 the reaction may be described by:

$$O(BT) + Ni(NiO) = V_0(BT) + V_{Ni}(NiO) + NiO \qquad (3)$$

For pure $BaTiO_3$ no other reactions occur. The reaction constant K_2 is then given by:

$$K_2 = (V_0(BT))\,(V_{Ni}(NiO)) = K_1 p_{O_2}^{-1/2} K_3 p_{O_2}^{1/2} = K_1 K_3 \qquad (4)$$

which is independent of p_{O_2}. There is no charge flow through any of the interfaces. All interface reactions are such that charge flow only occurs inside one homogeneous medium and as such is not of importance

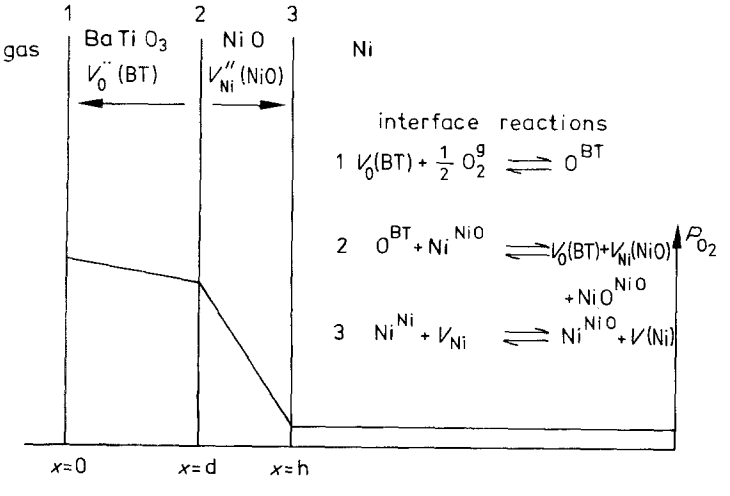

Figure 1 Schematic drawing of the ceramic–oxide–metal sequence, the directions of the diffusing species and the interface reactions.

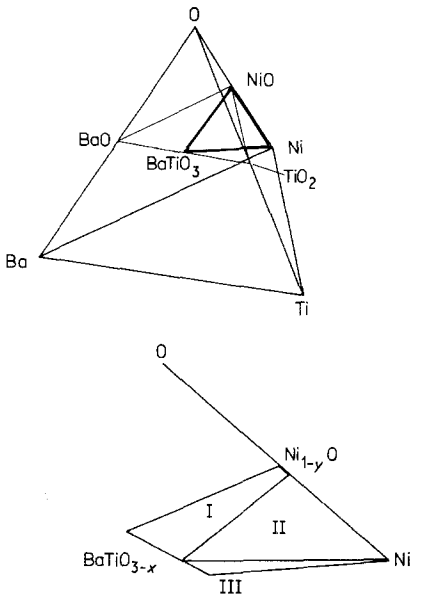

Figure 2 Schematic phase relations in the system $BaTiO_3$–NiO–Ni. I, $BaTiO_{3-x}$ + $Ni_{1-y}O$(+gas, $p_{O_2} > p^{eq}_{O_2}$); II, $BaTiO_{3-x}$ + $Ni_{1-y}O$ + Ni(+gas, $p_{O_2} = p^{eq}_{O_2}$); III, $BaTiO_{3-x}$ + Ni(+gas, $p_{O_2} < p^{eq}_{O_2}$).

for the interface reactions. Rate-controlling interface reactions show a linear time dependence [29], which is not observed here, excluding it from being a rate-controlling mechanism.

3.3. Diffusion processes

Before presenting the results of the studies aimed at the determination of the rate-controlling step, the defect chemistry involved in the diffusion in $BaTiO_3$ and NiO has to be discussed in further detail. The diffusion in $BaTiO_3$ proceeds by double positively charged oxygen vacancies, $\ddot{V}_O$(BT) [16, 17], as the fastest step. That in NiO shows diffusion by double negatively charged $\ddot{V}_{Ni}$(NiO) in a partial pressure range above about 10^{-5} bar [14] as the fastest step, for both Kroger Vink notations is used. These facts will be used later in so far as only these two species control diffusion, differently charged species giving different diffusion rates are excluded.

Fig. 3 shows the rate of oxidation observed in blank

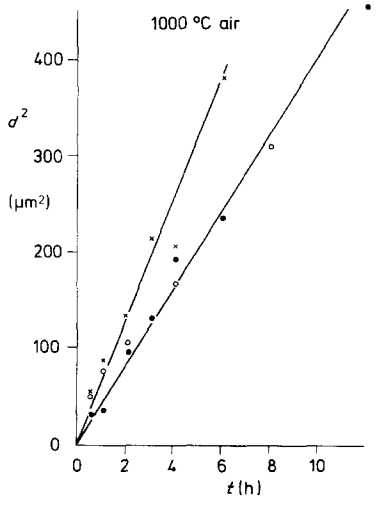

Figure 3 Rate of oxidation at 1000° C in air for blank and $BaTiO_3$ embedded nickel. (●) $BaTiO_3$ + Ni, (○) $BaTiO_3$(NbCo) + Ni, (x) blank nickel.

TABLE II Thickness of NiO layer formed under various conditions. For nickel embedded in pure $BaTiO_3$ the cover layer of $BaTiO_3$ was 4.5 mm thick

Temp. (° C)	Time (h)	Blank Ni, measured value		Embedded Ni, measured, d_{NiO} (μm)
		d_{NiO} (μm)	dG (wt %)	
700	2	0.8	–	2.0
	20	2.3	–	5.9
	50	3.4	–	8.0
	100	5.5	–	11.7
800	2	2.7	–	3.2
950	2	9.2	0.62	5.9
1000	0.5	7.2	0.54	5.4
1000	1.0	9.2	0.38	5.9
1000	2.0	11.5	0.85	9.7
1000	3.0	14.6	1.17	11.4
1000	4.0	14.3	0.95	13.9
1000	6.0	19.5	1.19	15.3
1000	12.0	–	–	21.3
1050	2.0	15.7	0.66	15.9
1100	2.0	–	–	16.8
1150	2.0	27.8	1.76	23.6
1200	2.0	–	–	16.8
1250	2.0	43.9	3.01	36.0
1300	0.5	13.3	–	13.5
1300	1.0	19.6	–	14.3
1300	1.5	23.5	–	19.3
1300	2.0	55.3	3.39	50.3
1300	3.0	63.3	–	52.7
1350	2.0	62.5	–	–
1400	2.0	78.4	–	–

nickel and in nickel embedded in $BaTiO_3$ at 1000° C in air. In both cases a parabolic, i.e. diffusion-controlled rate law is obeyed, that in the case of blank nickel is resembled by the weight change results. All measured values are listed in Table II. This indicates that at 1000° C diffusion through the NiO layer is the rate-controlling step. At 700 and 1300° C the parabolic rate law is not obeyed so well.

In order to check whether at different temperatures the pattern changes severely, an Arrhenius-

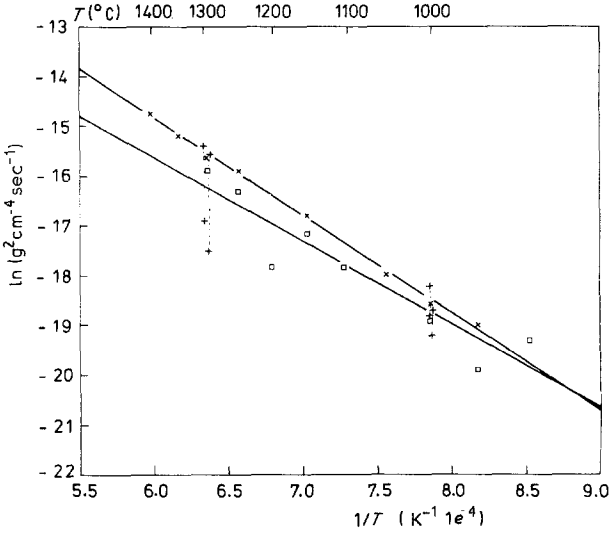

Figure 4 Arrhenius plot of the oxidation rate of (+) blank nickel and (□) $BaTiO_3$-embedded nickel between 950 and 1400° C (the values at 700 and 800° C are listed in Table II and not included here, due to the broad error margin).

type plot was made for blank and embedded nickel for the temperature range 900 to 1300° C, for blank nickel up to 1400° C. The results in Fig. 4 show, that between 950 and 1300° C a unique activation energy is observed (139.4 kJ mol^{-1} = 1.44 eV for embedded and 163.2 kJ mol^{-1} = 1.69 eV for blank nickel). In case different mechanisms because rate-controlling for the embedded nickel, deviations from the Arrhenius-type behaviour should occur. A comparison of known diffusion data for double positively charged oxygen vacancies in $BaTiO_3$ (D_{V_O} = 5700 exp (−23780.6/T (K)) cm^2 sec^{-1}) [16] and double negatively charged nickel vacancies in NiO ($D_{V_{Ni}}$ = 0.0164 exp (−11276.6/T(K)) cm^2 sec^{-1}) [14] shows: first, both values obtained for the activation energy lie in the range of values found for diffusion in NiO; second, according to the diffusion constants given above, below 700° C diffusion in $BaTiO_3$ becomes the slowest step due to the different activation energies in both diffusion constants. This, together with a larger percentage error margin at this low temperature explains the deviation from the parabolic behaviour and a deviation from the Arrhenius-type behaviour at this temperature.

These results show that for oxidizing heat treatment the diffusion in NiO (as desired) at a temperature of about 1000° C is the rate-controlling step. Thus the rate dependence would allow a fast oxidation of the ceramic with limited oxidation of nickel.

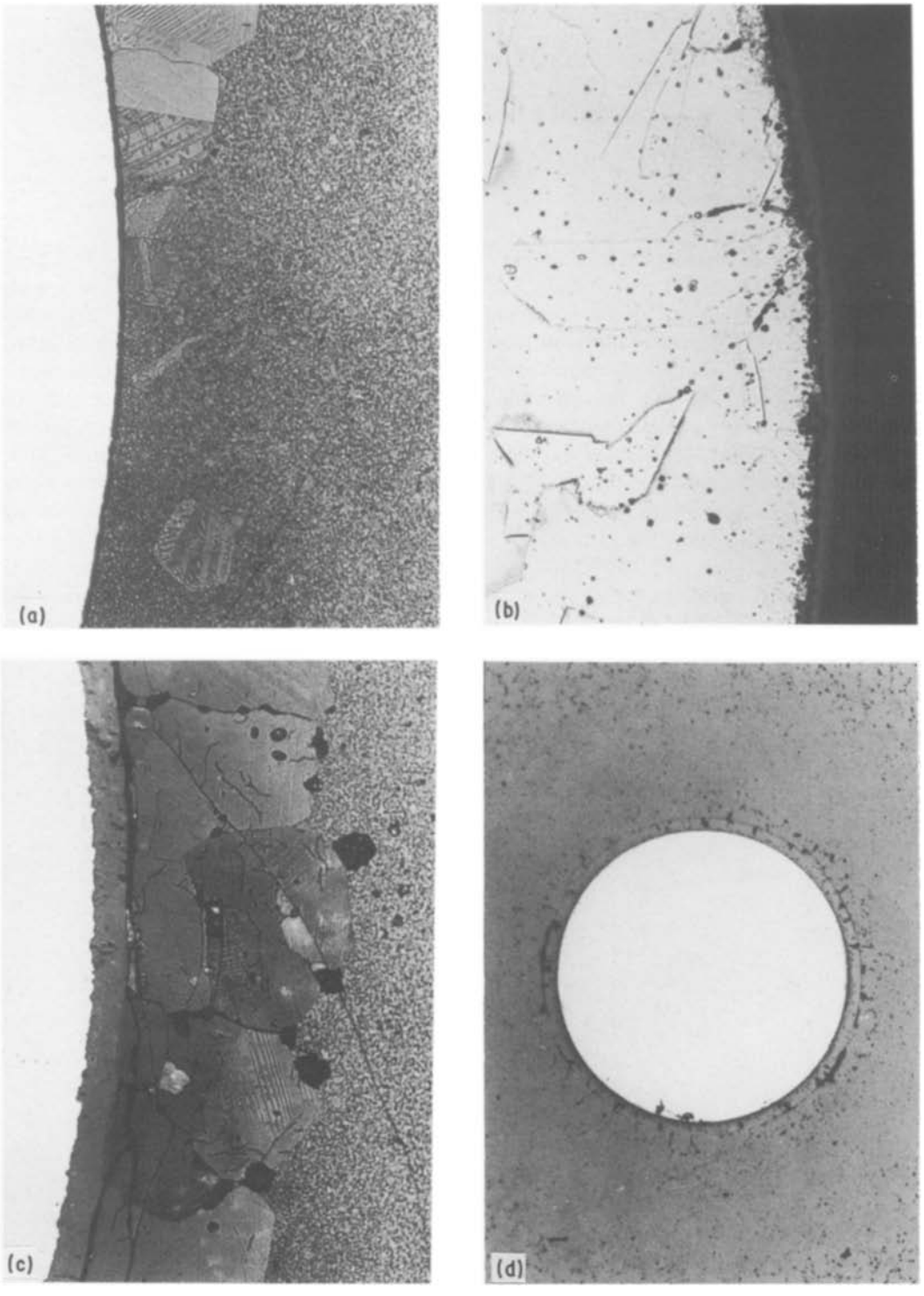

Figure 5 (a) $BaTiO_3$ + Ni as-sintered. × 500 etched, showing excessive grain growth in $BaTiO_3$. (b) Blank nickel oxidized 2 h at 700° C in air. (c) $BaTiO_3$ + Ni oxidized for 2 h at 100 0° C in air. (d) $BaTiO_3$ + Ni oxidized for 2 h at 1300° C in air. × 100

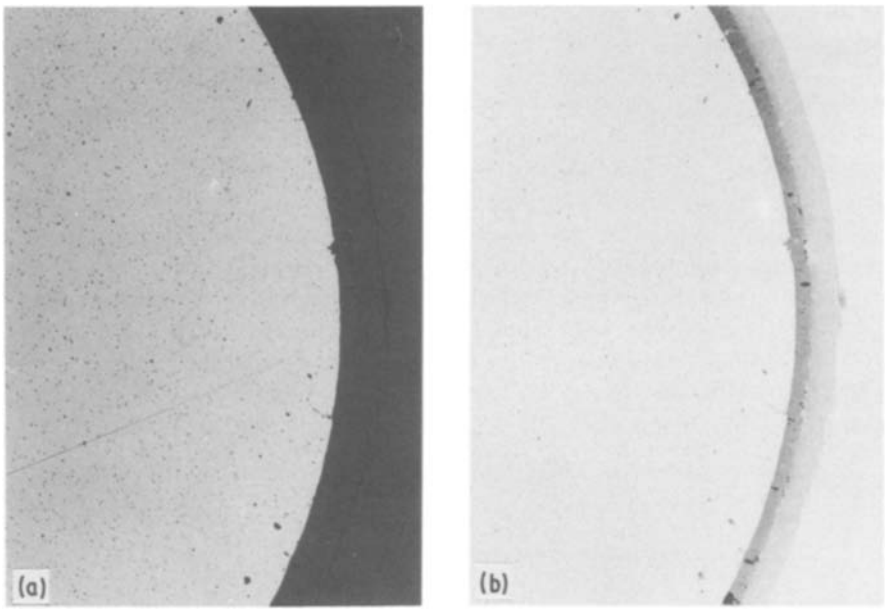

Figure 6 $BaTiO_3$ + Ni oxidized for 2 h at 1300° C in air. Two layers are visible in the NiO layer shown (a) under normal and (b) under polarized light. × 200

3.4. Morphology and composition of the NiO layer formed

Figs 5 to 9 show the morphology of the interface under various conditions: Fig. 5a shows the as-sintered stage, indicating that at the $BaTiO_3$ interface some grain growth occurs in pure $BaTiO_3$ due to differential sintering, which leads to an increase in pressure. Figs 5b, c and d show a NiO layer formed on blank and embedded nickel heat treated 2 h at 700, 1000 and 1300° C, respectively. While at 700° C interface 3 is rugged, it becomes smooth at higher temperatures. On the other hand, at temperatures above 1100° C the NiO layer shows a distinct porosity close to the same interface. This excludes any effect of geometry that could arise due to the fact that a planar geometry is no longer fulfilled, i.e. d_{NiO} is not longer much smaller than d_{Ni}, which is the diameter of the nickel wire. Under polarized light the NiO layer forms two distinct sublayers shown in Fig. 6. Etching of nickel reveals a low density of etch pits at 700° C and a high one at 1300° C, which shows that the vacancy concentration in nickel at interface 3 at a high temperature is higher than at lower temperatures shown in Figs 7a and b.

SEM images and maps together with microprobe scans reveal that no barium dissolves into NiO, while only up to 1 mol % NiO dissolves in $BaTiO_3$ as far as 20 μm from the interface. Fig. 8 shows such an interface with the corresponding maps for nickel and barium. Reducing such an NiO layer by an additional reducing heat treatment transforms all NiO back into nickel, where only a few micrometre sized $BaTiO_3$ particles are embedded in the reduced metallic nickel after reduction.

This simple pattern is altered completely, when instead of pure $BaTiO_3$, NbCo-doped $BaTiO_3$ is used. Already in the sintered state the nickel wire shows

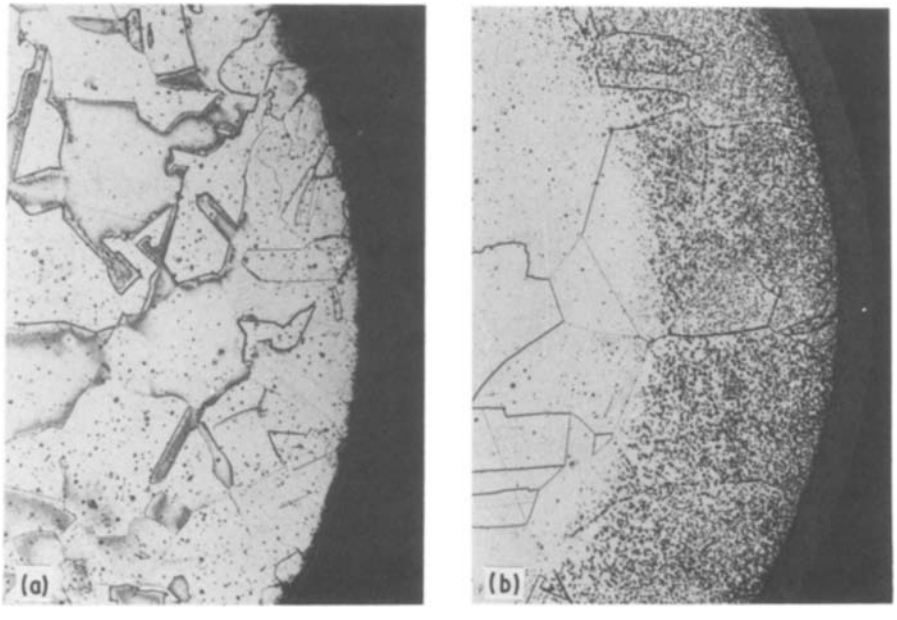

Figure 7 Blank nickel oxidized for 2 h at (a) 700° C and (b) 1300° C in air, showing a very different etch pit density in nickel. × 200

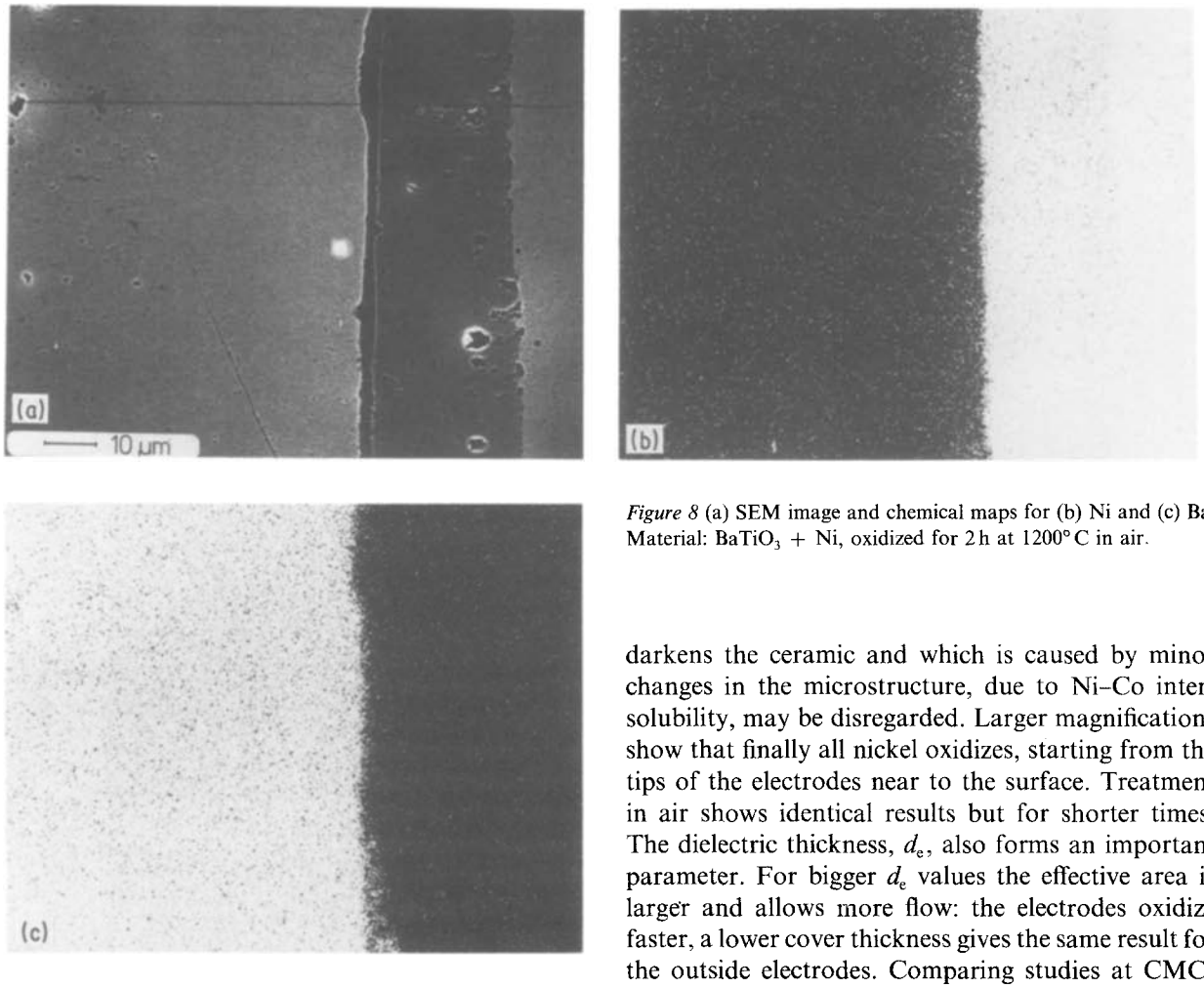

Figure 8 (a) SEM image and chemical maps for (b) Ni and (c) Ba. Material: $BaTiO_3$ + Ni, oxidized for 2 h at 1200° C in air.

distinct grain-boundary grooving even inside due to dissolution of cobalt. Upon oxidizing heat treatment, a very rugged oxide layer forms between $BaTiO_3$ and nickel. The nickel also shows inner oxidation due to the cobalt content. Fig. 9 shows the SEM image and maps for nickel, cobalt and oxygen showing the strong dissolution. Niobium was not found to enter into NiO or nickel. The oxidation rate in Fig. 3 shows that for short times deviations from the rate observed with pure $BaTiO_3$ occur. For longer times it approaches the latter, however. Because of the rugged interface, the evaluation of these data is more difficult and includes a broader error margin.

This shows that cobalt would not be a desirable dopant to be used in a $BaTiO_3$ ceramic in combination with nickel electrodes. The strong affinity of cobalt and nickel for each other is expressed by their high intersolubility in both the metallic and oxide states [25, 26]. The cobalt content in nickel has the consequence that the $p_{O_2}^{eq}$ of Equation 2 is shifted towards lower p_{O_2} values and the diffusivity of the oxide layer is strongly enhanced [32].

3.5. Effect of the multilayer geometry

Figs 10a to f show CMCs with nickel electrodes heat treated in N_2 (log p_{O_2} = −4.5 bar) at 1100° C for different lengths of time. The brightness of the ceramic indicates whether it is in a semiconducting (dark) or in an insulating (bright) state. It is well discernible, that the area between the electrodes remains dark even after longer times. Thereby a second effect which also darkens the ceramic and which is caused by minor changes in the microstructure, due to Ni–Co intersolubility, may be disregarded. Larger magnifications show that finally all nickel oxidizes, starting from the tips of the electrodes near to the surface. Treatment in air shows identical results but for shorter times. The dielectric thickness, d_e, also forms an important parameter. For bigger d_e values the effective area is larger and allows more flow: the electrodes oxidize faster, a lower cover thickness gives the same result for the outside electrodes. Comparing studies at CMCs without electrodes showed immediate transformation into the insulating state. As far as the cobalt dissolution in nickel and NiO is concerned, the results of NbCo-doped cylinders could be reproduced.

This shows that although the rate-controlling mechanisms seem to favour such a heat treatment, nickel acts as a strong sink. An estimation about the oxygen consumption of $BaTiO_3$ and that of nickel using d_e = 25 µm and an electrode thickness of 5 µm shows that the amount of oxygen necessary to oxidize nickel is two to three orders of magnitude larger than that to transform the ceramic into an insulating state. This fact, together with the geometry, which only allows subsequent oxidation (i.e. there is always blank nickel left), shows that no efficient oxidizing heat treatment with nickel electrodes is possible in multilayer capacitors.

4. Conclusion

The investigation of the use of an oxidizing second heat treatment of $BaTiO_3$ with nickel electrodes after reducing sintering shows the following results.

1. Nickel or NiO is stable with $BaTiO_3$ depending on the p_{O_2} of the gas atmosphere. As there is no solubility of either barium or titanium in NiO the equilibrium p_{O_2} of the reaction Ni + 0.5 O_2 = NiO forms the limit, whether nickel or NiO coexists with $BaTiO_3$.

2. The oxidation of nickel embedded in $BaTiO_3$ follows a parabolic rate, between 950 and 1300° C, and thereby indicates that diffusion in NiO is the rate-controlling step. At lower temperatures significant deviations from this behaviour occur.

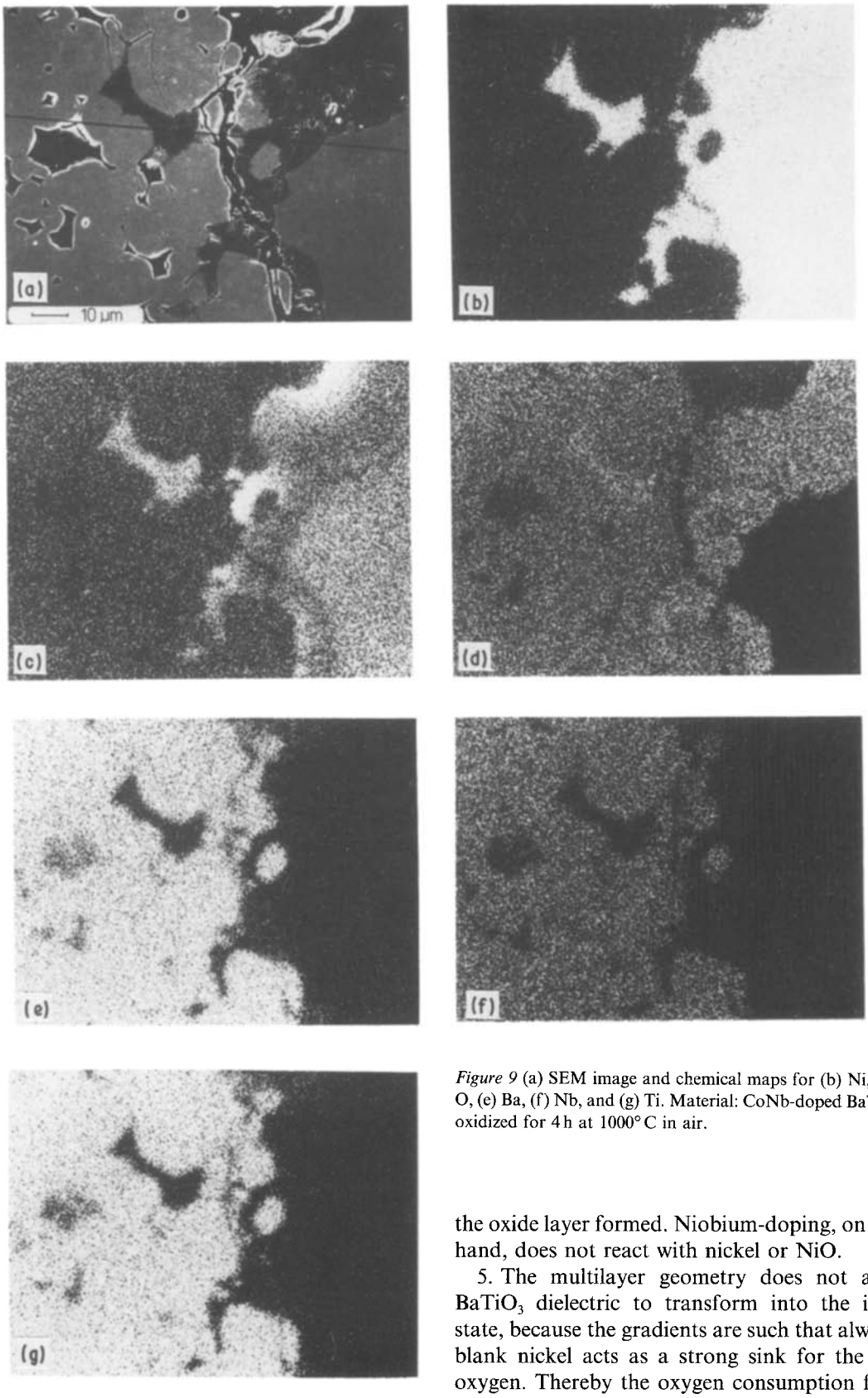

Figure 9 (a) SEM image and chemical maps for (b) Ni, (c) Co, (d) O, (e) Ba, (f) Nb, and (g) Ti. Material: CoNb-doped $BaTiO_3$ + Ni, oxidized for 4 h at 1000° C in air.

3. The reaction at the interface between $BaTiO_3$ and the newly formed NiO proceeds by the reaction

$$O(BT) + Ni(NiO) = V_0(BT) + V_{Ni}(NiO) + NiO$$

for which the reaction constant is independent of p_{O_2}.

4. Dopants in $BaTiO_3$ like cobalt alter the oxidation drastically: they dissolve in nickel and NiO considerably altering the oxidation rate and the morphology of the oxide layer formed. Niobium-doping, on the other hand, does not react with nickel or NiO.

5. The multilayer geometry does not allow the $BaTiO_3$ dielectric to transform into the insulating state, because the gradients are such that always some blank nickel acts as a strong sink for the diffusing oxygen. Thereby the oxygen consumption for nickel oxidation is two to three orders of magnitude larger than that necessary to transform the ceramic into the insulating state.

Acknowledgements

The author thanks Mr Groenewoud and Mrs Vervest, Elcoma Eindhoven for performing the microprobe analysis, Mr Herff for the optical microscopy and Mr Hünten for performing the heat treatments. Thanks are also due to Drs Wernicke, Hennings and Waser for their support and helpful discussions.

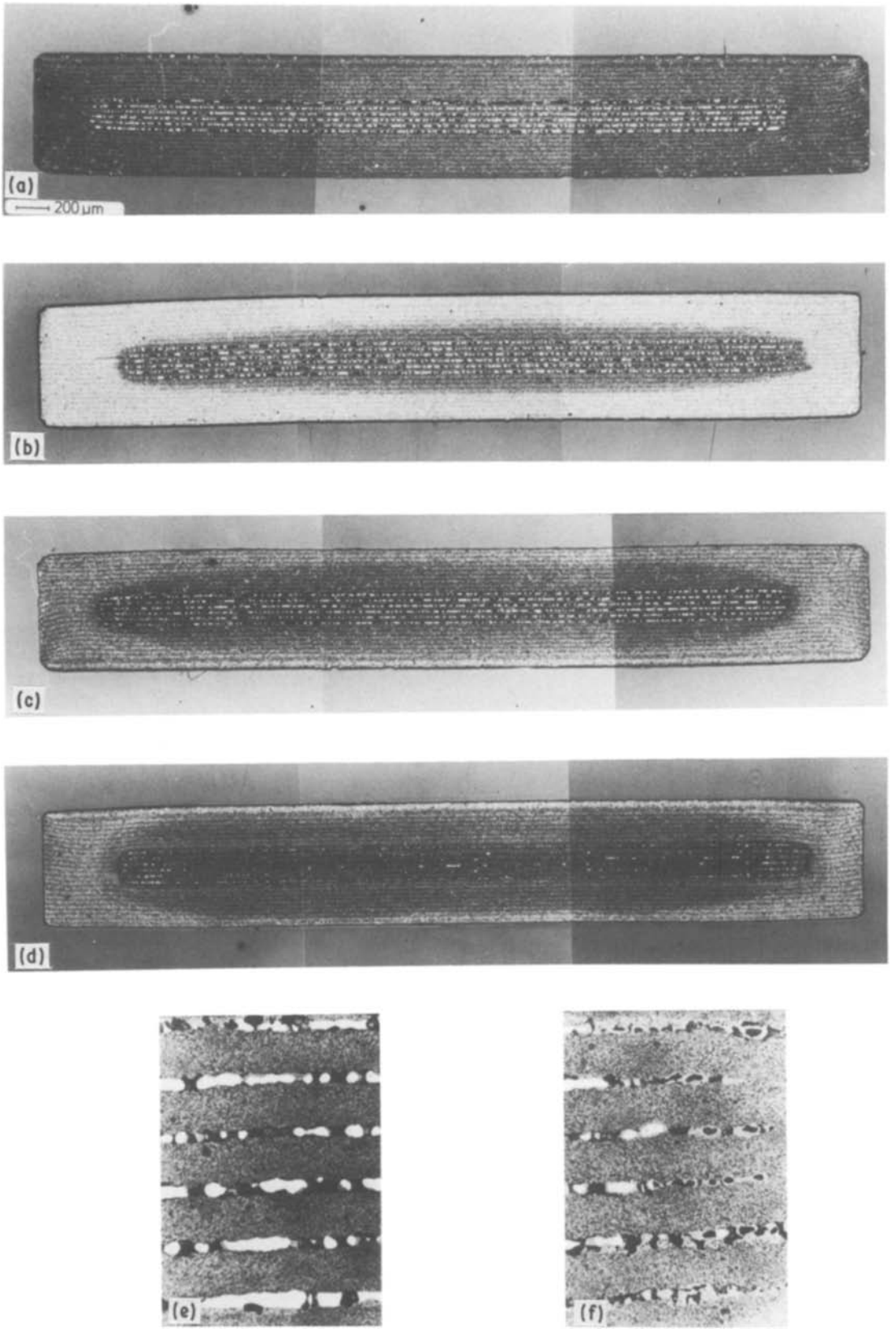

Figure 10 CMCs made from CoNb-doped $BaTiO_3$ with nickel electrodes, exposed to an oxidizing second heat treatment in N_2 (log $p_{O_2} = -4.5$ bar) at 1100° C. (a) As-sintered, (b) 2 h, (c) 10 h, (d) 100 h, (e) 50 h centre of the device, (f) tips of the electrodes, showing a different degree of oxidation.

References

1. J. DANIELS, K. H. HÄRDTL, D. HENNINGS and R. WERNICKE, *Philips Res. Rept.* **31** (1976) 487.
2. H. J. HAGEMANN and D. HENNINGS, *J. Amer. Ceram. Soc.* **64** (1981) 590.
3. N. H. CHAN, R. K. SHARMA and D. M. SMYTH, *ibid.* **65** (1982) 167.
4. N. H. CHAN and D. M. SMITH, *ibid.* **67** (1984) 285.
5. G. V. LEWIS and C. R. A. CATLOW, *J. Phys. Chem. Solids* **47** (1986) 89.
6. H. J. HAGEMANN, *Ferroelectrics* **22** (1978) 743.
7. *Idem, J. Phys. C Solid State Phys.* **11** (1978) 3333.
8. R. WASER, "Long term reliability of multilayer ceramic capacitors", contribution to: CARTS '87, 9–12 March, 1987, Anaheim, California.
9. W. LANGENHORST and R. WASER, *Electron. Compon.*

Applic. **8** (1986) 15.
10. K. E. VOLK, "Nickel und Nickellegierungen, Eigenschaften und Verhalten" (Springer Verlag, Berlin, 1970).
11. C. M. OSBURN and R. W. VEST, *J. Phys. Chem. Solids* **32** (1971) 1331.
12. G. H. MEIER and R. A. RAPP, *Z. Phys. Chem. N.F.* **74** (1971) 168.
13. S. PIZZINI and R. MORLOTTI, *J. Electrochem. Soc.* **114** (1967) 1179.
14. J. NOWOTNY and A. SADOVSKY, *J. Amer. Ceram. Soc.* **62** (1979) 24.
15. H. G. SOCKEL and B. ILSCHNER, *Z. Phys. Chem. N.F.* **74** (1971) 284.
16. R. WERNICKE, *Philips Res. Rept.* **31** (1976) 526.
17. C. SCHAFFRIN, *Phys. Status Solidi (a)* **35** (1976) 79.
18. M. L. VOLPE and J. REDDY, *J. Chem. Phys.* **53** (1970) 1117.
19. V. F. CAPOZZI, "Multilayer Ceramic Capacitor Materials and Manufacture" (Oxy Metal. Ind. Corp., Nutley, New Jersey, 1975).
20. I. BURN, *Bull. Amer. Ceram. Soc.* **50** (1971) 501.
21. D. TAYLOR, *Br. Ceram. Trans. J.* **83** (1984) 5.
22. *Idem, J. Br. Ceram. Soc.* **84** (1985) 181.
23. K. HAUFFE, "Reaktionen in und an festen Stoffen" (Springer-Verlag, Berlin, 1955).
24. R. S. ROTH, T. NEGAS and L. COOK, "Phase Diagrams for Ceramists" (American Ceramic Society, Columbus, Ohio) Figs 53, 138, 205.
25. M. HANSEN and K. ANDERKO, "Constitution of binary alloys", (McGraw-Hill, New York, 1958).
26. T. NEGAS, R. S. ROTH, H. S. PARKER and D. MINOR, *J. Solid State Chem.* **9** (1974) 297.
27. J. J. RITTER, R. S. ROTH and J. E. BLENDELL, *J. Amer. Ceram. Soc.* **69** (1986) 155.
28. K. FUEKE and J. B. WAGNER, *J. Electrochem. Soc.* **112** (1965) 384.
29. H. SCHMALZRIED, "Festkörperreaktionen" (Verlag Chemie, Weinheim, Bergstrasse, 1971).
30. M. BACKHAUS-RICOULT, *Ber. Bunsenges. Phys. Chem.* **90** (1986) 684.
31. I. GOLECKI, R. L. MADDOX, H. L. GLASS, A. L. LIN, T. J. RAAB and H. M. MANASEVIT, *J. Electron. Mater.* **14** (1985) 531.
32. N. L. PETERSON and W. K. CHEN, "Diffusion mechanisms in transition metal oxides", invited paper at the International Conference on High temperature corrosion", March 1981, San Diego, California.

Received 29 June
and accepted 22 September 1987